DOI: 10.3190/jgeosci.270

Appendix A

A1 The high-grade terranes of the Moldanubian Zone

The high-grade belts of the Moldanubian Zone involve three lithotectonic units denoted as the Gföhl, Ostrong and Drosendorf assemblages (Figs 2 and 3). The belts developed during the NW–SE shortening of the Moldanubian Zone between 350 and 335 Ma. They embrace the central Moldanubian antiform, occupied by the South Bohemian Batholith, and trend into the Sudetes Mts. region. Within the belts, a number of mafic to intermediate, strongly potassic to ultrapotassic plutonic bodies occur in a close spatial association with high-pressure (HP) to ultra-high pressure (UHP) granulites (Janoušek and Holub 2007; Lexa et al. 2011). Occurrence of abundant (U)HP granulites and garnet-bearing meta-peridotites indicates their exposure to upper-mantle conditions.

The (U)HP rocks of the Gföhl Assemblage overlie the Proterozoic to Early Paleozoic LP–HT grade Ostrong (Monotonous Group) and Drosendorf (Variegated Group) assemblages – see Fuchs (1976), Franke (2000) and Finger et al. (2007). The Gföhl Unit includes high-grade migmatitic gneisses with numerous bodies of (U)HP granulites, migmatized granite gneisses, high-temperature eclogites and mantle peridotites (Konopásek 2011; Žák et al. 2014). The Gföhl Assemblage has been considered the orogenic lower crust (Schulmann et al. 2014). Both belts include major ultrapotassic (durbachite) intrusions (Janoušek and Holub 2007) that intruded at *c.* 340–335 Ma, i.e. during the Variscan Moravo–Moldanubian tectono-metamorphic phase *sensu* Finger et al. (2007).

The high-grade rocks of the Gföhl Assemblage in both belts prevailingly overlay those of the lower grade Drosendorf Assemblage. Therefore, they were often considered nappes that

formed on the flanks of the central northeast-trending Moldanubian antiform (e.g. Matte et al. 1990; Fritz et al. 1996; Franke and Żelaźniewicz 2000). Many anatectic plutons of mostly granitic to granodioritic compositions penetrated the Moldanubian metamorphic units between the two belts, forming the so-called South Bohemian Batholith (SBB) (Fig. 2). Most granitic intrusions of the SBB have been dated at 321–323 Ma, while the granodiorite plutons intruded later, at 319–315 Ma (e.g. Schulmann et al. 2009).

The western belt represents a transpression zone thermally softened due to the CBPC magmatism. The high-grade Moldanubian rocks are assumed to be exhumed at ~340 Ma (Žák et al. 2005; Faryad et al. 2013). As to the eastern belt, two contrasting concepts of the thrusting of Moldanubian Unit over Brunia were proposed.

(i) The Gföhl Unit is commonly interpreted as a low-angle, far-travelled, east-vergent thrust sheet thrusted over the mid-crustal rocks of the Variegated and Monotonous groups (e.g., Suess 1918; Thiele 1976; Matte 1986; Franke 1989). The different opinions concern the origin and formation of the Gföhl Assemblage. Fuchs (1976) interpreted it as a nappe, having localized its root at the eastern margin of the Moldanubian Zone and assumed its initial thrusting to the west – see also Kachlík (1999), Franke (2000) and Medaris et al. (2006). Finger et al. (2007) discussed a tectonic scenario with two distinct tectono-metamorphic phases, the Moravo–Moldanubian (345–330 Ma) and Bavarian (330–315 Ma). During the first phase, the authors also assumed the reverse east-to-west thrusting of the HP–HT metamorphic rocks. The Teplá–Barrandian block was considered as a rigid backstop along which the subducted HP–HT rocks were steeply exhumed.

(ii) Alternatively, Schulmann et al. (2009, 2014) considered eastward underplating of the TBU and MLD and extrusion of the Saxothuringian-derived rocks with the Brunia Block acting as a rigid back-stop. This view was based on a number of studies modeling the

vertical mass extrusions caused by E–W compression to explain the juxtaposition of the mid- and lower crustal rocks observed in the Moldanubian Zone (Štípská et al. 2004; Schulmann et al. 2005, 2008; Hasalová et al. 2008). In this context, the term 'Gföhl Assemblage' was proposed to replace 'Gföhl Unit' previously considered as part of a single (Gföhl) nappe (Finger et al. 2007; Faryad and Kachlík 2013; Žák et al. 2014).

Štípská et al. (2004) suggested that the Orlica–Śnieżnik Dome might be a result of combined vertical extrusion and lateral flow during syn-convergent exhumation. Schulmann et al. (2005) studied the central part of the Moldanubian–Brunia collisional margin. They interpreted the internal lower crustal belt as a large-scale, 20 km wide extrusion that was thrust in a bivergent manner over the middle crustal synclines. The concept of two sub-vertical extrusions derived from the lower crust and then laterally spread over the middle crust is close to the original idea of the autochthonous nature of lower-crustal nappes (Suess 1918; Fuchs 1976).

A2 A short description of the DRTG method

The only assumption of the DRTG method is that the refraction data exist, i.e., velocities of elastic waves prevailingly increase with the depth. Then, the rays corresponding to recorded surface-to-surface refraction waves have at least one turning point (with a horizontal direction) separating their descending and ascending paths. Let's specify probe refraction rays G_m to bottom at single grid points *m*. Fig. A1 illustrates such a system of the probe refraction rays that is suitable for the calculation of unknown corrections. In the case of 2-D data, the azimuth of seismic line gives the ray azimuth. Originally (Novotný 1981), the method derived a 2-D velocity distribution starting from a 1-D model. It was extended to 2-D starting models which are necessary for iterative refinements. Here, the theory involving the 3-D version is presented as described in Novotný et al. (2009, pp 594–597). The refraction data along a profile line, however, allow only the 2-D velocity inversion.

The basic linearization equation used in refraction tomographies operates with the slowness function s(x,y,z) that is reciprocal to the velocity distribution v(x,y,z), i.e.,

$$s(x,y,z) = 1/v(x,y,z). \tag{A1}$$

Assume a starting slowness model $s_o(x,y,z)$ that is close to the searched final model

$$s(x,y,z) = s_0(x,y,z) + \Delta s(x,y,z), \tag{A2}$$

i.e., using the L2 norm,

$$\left\| s(x,y,z) - s_0(x,y,z) \right\| = \left\| \Delta s(x,y,z) \right\| \approx 0 \ . \tag{A3}$$

Then, the following well-known linear relation between the total time difference Δt and the slowness differences $\Delta s(x,y,z)$ along a particular ray G_m is valid:

$$\Delta t(G_m) \approx \int_{G_m} \Delta s(x,y,z)\, dg \ . \tag{A4}$$

Integrating runs along the ray G_m established for the starting model $s_o(x,y,z)$. The integral time discrepancy $\Delta t(G_m)$ in (A4) then denotes the difference between the input (observed) and ray (calculated) time due to the $s_o(x,y,z)$ starting model. The linear equation (A4) can be used to find the slowness corrections $\Delta s(x,y,z)$ to the $s_o(x,y,z)$ model. After introducing them by means of (A2), an updated model is obtained. As a rule, one model update is not sufficient because of the linearization errors of the approximation (A4). To reduce them and concurrently to verify the searched final model, several iterations with starting models updated in this way must be applied.

A numerical depth-recursive algorithm for unknown slowness differences $\Delta s(x,y,z)$ can be easily obtained if their calculations proceed consecutively in the depth steps of the model grid sampling, i.e., z_0, z_1, z_2, … . In the i-th step, the grid slowness corrections $\Delta s(x_j,y_k,z)$ are then established at all upper grid nodes including the z_i depth, i.e., for $z \le z_i$. Now, calculate the slowness differences at the next z_{i+1} level. Consider the refraction rays $G^{i+1}{}_m$ crossing the plane $z = z_i$ and bottoming on this depth level $z = z_{i+1}$. Divide the integration into two parts involving $G^{i+1}{}_m$ above and beneath the level z_i, i.e.,

$$\Delta t\left(G^{i+1}{}_m, z_o, z_i\right) = \Delta t\left(G^{i+1}{}_m\right) - \int\limits_{z_0 \le z \le z_i} \Delta s(x,y,z)\,dg = \int\limits_{z > z_i} \Delta s(x,y,z)\,dg \qquad \text{(A5)}$$

The integration of $\mathbf{\Delta}t(G^{i+1}{}_m,z_o,z_i)$ down to $z \le z_i$ involves the already known corrections Δs (see full grid nodes in Fig. A1). This integration comprises both branches of the refraction ray path G_m from the surface to the horizontal grid plane $z=z_i$ (Fig. A1). The term $\mathbf{\Delta}t(G^{i+1}{}_m,z_o,z_i)$ obviously denotes the time differences at the single *m* nodes extrapolated from $z=z_o$ downward to the depth level $z=z_i$.

The probe refraction rays G_m (called simply the grid rays) may be computed by any shooting ray-tracing procedure initiating their calculations at the corresponding grid node (the ray bottom) under two mutually opposite, horizontal directions (Fig. A1). The emergence points E_1 and E_2, if they exist, define the hypothetical source and receiver points due to a probe ray G_m with their corresponding offset *q* and midpoint position *p*. Naturally, not all grid rays reach the surface or have the emergence points compatible with the available data. As well, their trajectories differ during iterations in dependence on the starting model used. However, more iterations with the grid rays recalculated for the updated velocity models allow reaching the required fit between the observed and model travel times. An advantage of DRTG method is that it evaluates the travel-time fit (td) specifically at every model node. Figure A2 illustrates the bottoms of successful (a) and irregular (b) grid rays calculated for the CEL09 profile in Novotný (2011).

In the i+1 step of depth recursion, the grid rays G_m bottoming at all grid nodes on $z=z_{i+1}$ are calculated. The E1, E2 emergence points of a successful G_m ray determine the offset *q* and midpoint coordinate *p* corresponding to its *ray* travel time. By the use of a suitable numerical representation (Appendix B), the *observed* travel-time for *q,p* required is interpolated.

The DRTG algorithm applies certain criteria eliminating irregular rays and the rays beyond the available data range. The subset of the grid rays G_m with successfully interpolated field travel times are then used to determinate the model corrections at all grid levels. The relation (A5) between the time misfits Δt extrapolated downward to $z=z_i$ and slowness corrections Δs at the next depth level $z=z_{i+1}$ is used for the proper numerical implementation of the DRTG algorithm described below. It is based on the linear spline functions (Novotný et

al. 2009). Note that integration in (A5) involves just the deepest bottoming part of the $G^{i+1}{}_m$ ray path between the z_i and z_{i+1} levels.

Expand the Δs function among the grid nodes using the linear spline functions (Fig. A3),

$$\Delta s(x,y,z) = \sum_{j,k,l} \Delta s(x_j, y_k, z_l)\, X_j(x)\, Y_k(y)\, Z_l(z) \tag{A6}$$

where the spikes, e.g. $Z_l(z)$, are defined as

$$Z_l(z) = \begin{cases} (z - z_{l-1}) / (z_l - z_{l-1}), & \text{for } z_{l-1} < z \le z_l, \\ (z_{l+1} - z) / (z_{l+1} - z_l), & \text{for } z_l \le z < z_{l+1}, \\ 0, & \text{elsewhere.} \end{cases} \tag{A7}$$

Substituting (A6) into the right-hand side integral (A5) and writing down the non-zero terms for l=i and l=i+1, one gets a system of linear equations for unknown grid values $\Delta s(x_j,y_k,z_{i+1})$ in the plane z_{i+1},

$$\Delta t\left(G^{i+1}{}_m, z_o, z_i\right) = C_m + \sum_{j,k} D_{\mathbf{jkm}} \Delta s(x_j, y_k, z_{i+1}), \tag{A8}$$

where

$$C_m = (z_{i+1} - z_i)^{-1} \sum_{j,k} \Delta s(x_j, y_k, z_i) \int_{z_i \le z \le z_{i+1}} X_j(x) Y_k(y) (z_{i+1} - z)\, dg_m, \tag{A9}$$

$$D_{\mathbf{jkm}} = (z_{i+1} - z_i)^{-1} \int_{z_i \le z \le z_{i+1}} X_j(x) Y_k(y) (z - z_i)\, dg_m. \tag{A10}$$

j,k run over all grid points of the planes $z = z_i$ and $z = z_{i+1}$. Note that non-zero contributions to integrations (A9) and (A10) come from the grid points closest to the raypath $G^{i+1}{}_m$ (Fig. A3). The vector $\mathbf{C_m}$ and the interpolation matrices $D_{\mathbf{jkm}}$ correspond subsequently (m=1, 2, …, M) to the engaged (j_m,k_m) grid points at the grid plane $z=z_{i+1}$. The computation of $\Delta t(G^{i+1}{}_m,z_o,z_i)$ according to (A5) and (A8) involves all the slowness differences $\Delta s(x_j,y_k,z_l)$ mapped out in the previous depth recursions l=1,2,…, i:

$$\Delta t\left(G^{i+1}{}_m, z_o, z_i\right) = \Delta t\left(G^{i+1}{}_m\right) - \sum_{j,k,l} \Delta s(x_j, y_k, z_l) \int\limits_{z_0 \le z \le z_i} X_j(x)\, Y_k(y)\, Z_l(z)\, dg_m \,. \quad \text{(A11)}$$

In the numerical implementation of the DRTG algorithm, the integrations in (A8–11) are performed in the time steps used for the ray-path computation.

Direct inversion method

The simplest computational scheme for obtaining the unknown $\Delta s(x_j,y_k,z_{i+1})$ in (A8) can be derived for the grid step Δz much smaller than Δx, Δy. It allows neglecting the x and y variability near the individual ray bottoms at the $z=z_{i+1}$ plane used for velocity inversion. Then, a common fixed value $\Delta s_m(z_{i+1})$ may be used in the sum (A8) instead of $\Delta s(x_j,y_k,z_{i+1})$, i.e.,

$$\Delta t\left(G^{i+1}{}_m, z_o, z_i\right) \approx C_m + \Delta s_m(z_{i+1}) \sum_{j,k} D_{jkm} \quad \text{(A12)}$$

or

$$\Delta s_m(z_{i+1}) \approx \left[\Delta t\left(G^{i+1}{}_m, z_o, z_i\right) - C_m\right] / A_m \quad \text{(A13)}$$

with A_m denoting the sum

$$A_m = \sum_{j,k} D_{jkm} \,. \quad \text{(A14)}$$

According to (A13), one $\Delta s_m(z_{i+1})$ correction can be derived from one downward-extrapolated value of Δt for the raypath $G^{i+1}{}_m$. This property implied the name of the method as “DIrect Inversion MEthod” (DIME). Thus, starting with i=1,2,… the equation (A13) can be used for recursive calculation of all tomographic corrections $\Delta s(x_j,y_k,z_{i+1})$ for updating the next slowness model

$$s\left(x_j, y_k, z_{i+1}\right) = s_o\left(x_j, y_k, z_{i+1}\right) + \Delta s\left(x_j, y_k, z_{i+1}\right) \quad \text{(A15)}$$

A numerical implementation of refraction inversion, based on the above relations, was performed and named as the DRTG method (Depth-Recursive Tomography in Grid). This method belongs to a wider family of direct inversion geophysical methods (Sen and Stoffa 2013). As proven by numerical tests (Novotný 2011, p. 846), a good accuracy of the DIME solver is attained for $\Delta z/\Delta x \leq 0.1$.

As follows from the above derivation, the proper velocity inversion based on (A8) or (A13) involves just the deepest bottoming part of imaging rays approaching to horizontal direction. Thus, the DRTG method establishes the velocities of engaged elastic waves rather for horizontal directions than for vertical ones. These velocities can substantially differ in the case of anisotropic behavior of studied medium as demonstrated by Novotný et al. (2009, pp 579–582).

References

FARYAD SW, KACHLÍK V (2013) New evidence of blueschist facies rocks and their geotectonic implication for Variscan suture(s) in the Bohemian Massif. J Metamorph Geol 31: 63–82

FARYAD SW, JEDLIČKA R, COLLETT S (2013) Eclogite facies rocks of the Monotonous Unit, clue to Variscan suture in the Moldanubian Zone (Bohemian Massif). Lithos 179: 353–363

FINGER F, GERDES A, JANOUŠEK V, RENÉ M, RIEGLER G (2007) Resolving the Variscan evolution of the Moldanubian sector of the Bohemian Massif: the significance of the Bavarian and the Moravo–Moldanubian tectonometamorphic phases. J Geosci 52: 9–28

FRANKE W (1989) Tectonostratigraphic units in the Variscan belt of Central Europe. In: DALLMEYER RD (ed) Terranes in the Circum–Atlantic Paleozoic Orogens. Geological Society of America, Special Papers 230: 67–90

FRANKE W (2000) The mid-European segment of the Variscides: tectonostratigraphic units, terrane boundaries and plate tectonic evolution. In: FRANKE W, HAAK V, ONCKEN O, TANNER D (eds) Orogenic Processes: Quantification and Modelling in the Variscan Belt. Geological Society, London, Special Publications 179: 35–61

FRANKE W, ŻELAŹNIEWICZ A (2000) The eastern termination of the Variscides: terrane correlation and kinematic evolution. In: FRANKE W, HAAK V, ONCKEN O, TANNER D (eds) Orogenic Processes: Quantification and Modelling in the Variscan Belt. Geological Society, London, Special Publications 179: 63–86

FRITZ H, DALLMEYER RD, NEUBAUER F (1996) Thick-skinned versus thin-skinned thrusting: rheology controlled thrust propagation in the Variscan collisional belt (the southeastern Bohemian Massif, Czech Republic–Austria). Tectonics 6: 1389–1413

FUCHS G (1976) Zur Entwicklung der Böhmischen Masse. Jb Geol B–A 129: 41–49

HASALOVÁ P, SCHULMANN K, LEXA O, ŠTÍPSKÁ P, HROUDA F, ULRICH S, HALODA J, TÝCOVÁ P (2008) Origin of migmatites by deformation-enhanced melt infiltration of orthogneiss: a new model based on quantitative microstructural analysis. J Metamorph Geol 26: 29–53

JANOUŠEK V, HOLUB F (2007) The causal link between HP/HT metamorphism and ultrapotassic magmatism in collisional orogens: case study from the Moldanubian Zone of the Bohemian Massif. Proc Geol Assoc 118: 75–86

KACHLÍK V (1999) Relationship between Moldanubicum, the Kutná Hora Crystalline Unit and Bohemicum (Central Bohemia, Czech Republic): a result of the polyphase Variscan nappe tectonics. J Czech Geol Soc 44: 201–291

KONOPÁSEK J (2011) Tectonic position of eclogites and blueschists in the Bohemian Massif. Geolines 23: 11–17

LEXA O, SCHULMANN K, JANOUŠEK V, ŠTÍPSKÁ P, GUY A, RACEK M (2011) Heat sources and trigger mechanisms of exhumation of HP granulites in Variscan orogenic root. J Metamorph Geol 29: 79–102

MATTE P (1986) Tectonics and plate tectonics model for the Variscan belt of Europe. Tectonophysics 126: 329–374

MATTE P, MALUSKI H, RAJLICH P, FRANKE W (1990) Terrane boundaries in the Bohemian Massif: result of large-scale Variscan shearing. Tectonophysics 177: 151–170

MEDARIS LG JR, BRIAN L. BEARD BL, JELÍNEK E (2006) Mantle-derived, UHP garnet pyroxenite and eclogite in the Moldanubian Gföhl nappe, Bohemian Massif: a geochemical review, new P–T determinations, and tectonic interpretation. Int Geol Rev 48: 765–777

NOVOTNÝ M (1981) Two methods of solving the linearized two-dimensional inverse seismic kinematic problem. J Geophys 50: 7–15

NOVOTNÝ M (2011) Depth-recursive tomography of Bohemian Massif at CEL09 transect – part A: deblurring of velocity image and resolution estimates. Surv Geophys 32: 827–855

NOVOTNÝ M, SKÁCELOVÁ Z, MRLINA J, MLČOCH B, RŮŽEK B (2009) Depth-recursive tomography along the Eger Rift using the S01 profile refraction data: tested at the KTB super drilling hole, structural interpretation supported by magnetic, gravity and petrophysical data. Surv Geophys 30: 561–600

SCHULMANN K, KRÖNER A, HEGNER E, WENDT L, KONOPÁSEK J, LEXA O, ŠTÍPSKÁ P (2005) Chronological constraints on the pre-orogenic history, burial and exhumation of deep-seated rocks along the eastern margin of the Variscan Orogen, Bohemian Massif, Czech Republic. Amer J Sci 305: 407–448

SCHULMANN K, LEXA O, ŠTÍPSKÁ P, RACEK M, TAJČMANOVÁ L, KONOPÁSEK J, EDEL JB, PESCHLER A, LEHMANN J (2008) Vertical extrusion and horizontal channel flow of orogenic lower crust: key exhumation mechanisms in large hot orogens? J Metamorph Geol 26: 273–297

SCHULMANN K, KONOPÁSEK J, JANOUŠEK V, LEXA O, LARDEAUX JM, EDEL JB, ŠTÍPSKÁ P ULRICH S (2009) An Andean type Palaeozoic convergence in the Bohemian Massif. C R Geosci 341: 266–286

SCHULMANN K, LEXA O, JANOUŠEK V, LARDEAUX JM, EDEL JB (2014) Anatomy of a diffuse cryptic suture zone: an example from the Bohemian Massif, European Variscides. Geology 42: 275–278

SEN MK, STOFFA PL (2013) Global Optimization Methods in Geophysical Inversion. Cambridge University Press, New York, pp 24–28

SUESS FE (1918) Bemerkungen zur neueren Literatur über die Moravischen Fenster. Mitt Geol Gesell 11: 71–128

ŠTÍPSKÁ P, SCHULMANN K, KRÖNER A (2004) Vertical extrusion and middle crustal spreading of omphacite granulite: a model of syn-convergent exhumation (Bohemian Massif, Czech Republic). J Metamorph Geol 22: 179–198

THIELE O (1976) Ein westvergenter kaledonischer Deckenbau in niederosterreichischen Waldviertel. Jb Geol B–A 119: 75–81

ŽÁK J, HOLUB FV, VERNER K (2005) Tectonic evolution of a continental magmatic arc from transpression in the upper crust to exhumation of mid-crustal orogenic root recorded by episodically emplaced plutons: the Central Bohemian Plutonic Complex (Bohemian Massif). Int J Earth Sci (Geol Rundsch) 94: 385–400

ŽÁK J, VERNER K, JANOUŠEK V, HOLUB FV, KACHLÍK V, FINGER F, HAJNÁ J, TOMEK F, VONDROVIC L, TRUBAČ J (2014) A plate-kinematic model for the assembly of the Bohemian Massif constrained by structural relationships around granitoid plutons. In: SCHULMANN K, MARTÍNEZ CATALÁN JR, LARDEAUX JM, JANOUŠEK V, OGGIANO G (eds) The Variscan Orogeny: Extent, Time Scale and the Formation of the European Crust. Geological Society, London, Special Publications 405: 169–196

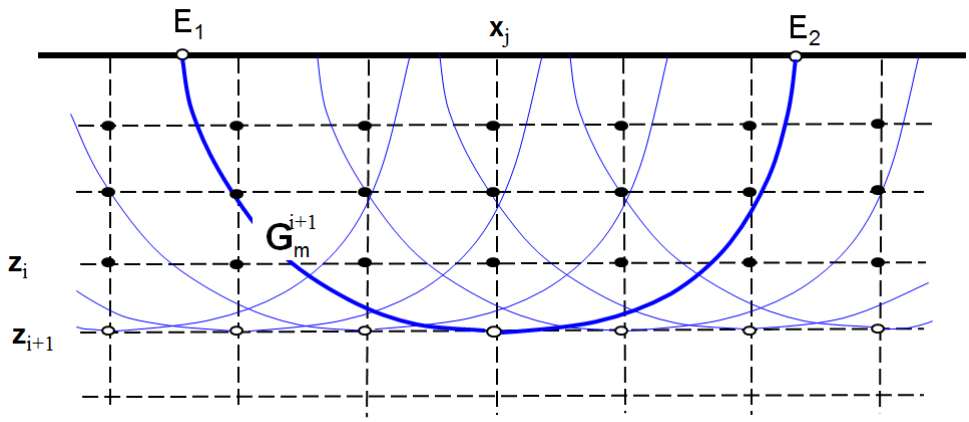

Fig. A1 The probe grid rays bottoming at the z_{i+1} grid level.

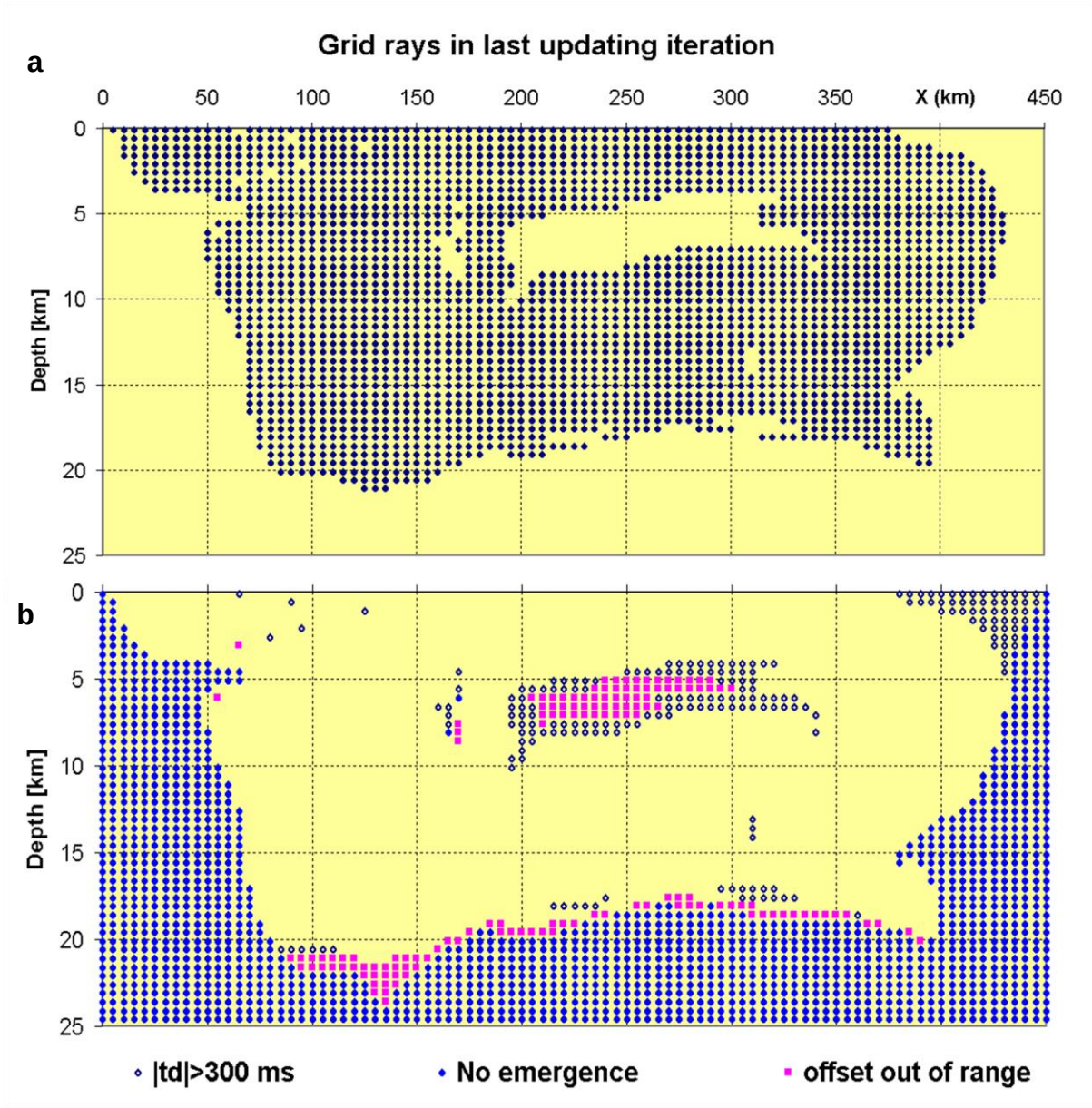

Fig. A2 a – Bottom points of successful grid rays used in the last updating iteration. **b** – Rejected grid rays according to the criteria applied. The missing corrections are interpolated from the adjacent valid values.

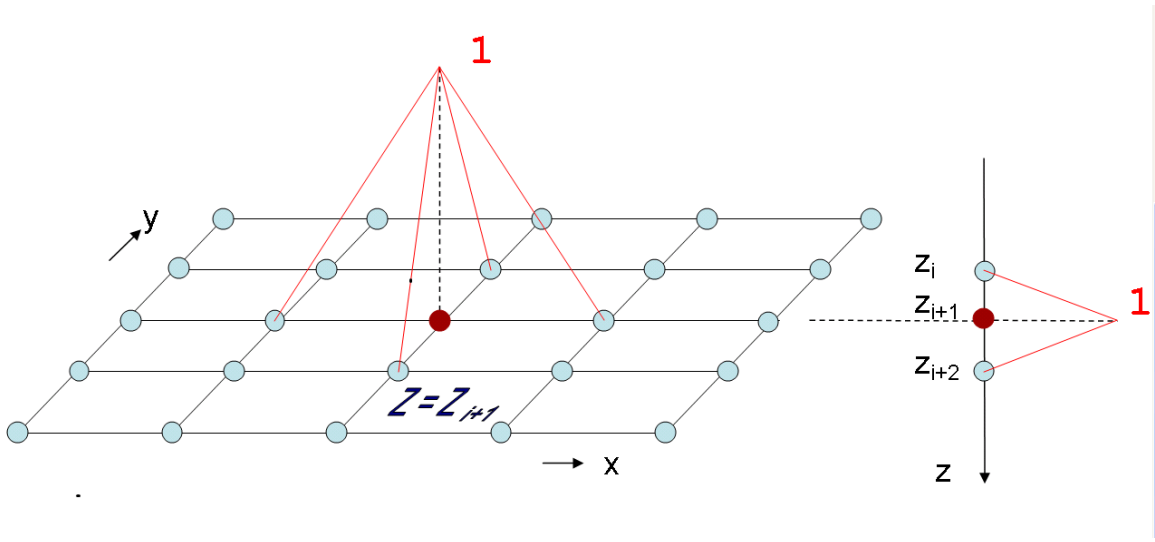

Fig. A3 The linear spikes used in the depth-recursive tomography.